Effects of Earth Encounters on the Physical Properties of Near-Earth Objects

by

Ho Chit Siu

Submitted to the Department of Earth, Atmospheric, and Planetary Sciences

in Partial Fulfillment of the Requirement for the Degree of

Bachelor of Science

at the

Massachusetts Institute of Technology

June 2014

Author _____

Ho Chit Siu

Department of Aeronautics and Astronautics

May 9, 2014

Certified by _____

Professor Richard P. Binzel

Thesis Supervisor

Certified by _____

Dr. Nicholas A. Moskovitz

Thesis Supervisor

Accepted by _____

Professor Richard P. Binzel

Chairman, Undergraduate Thesis Committee

Contents

Abstract

The effects of Earth encounters on the physical properties of near-Earth objects (NEOs) have been shown to be significant factors in their evolution. Previous studies have examined the effects of these encounters on reflectance spectra based on observational measurements, and effects such as spin state and shape changes have been studied in specific asteroids and in simulation. In this project, an automated light curve fitting routine was developed to support data reduction in an ongoing NEO survey. Additionally, data from previous NEO surveys were used to support simulation results by showing with a significant and highly differences between encounter and non-encounter populations' rotational frequency distributions, demonstrating that Earth encounters do have an effect on asteroid rotational frequencies by increasing the overall frequency as well as causing a wider distribution of frequencies when compared to non-encounter populations. These data were, however, unable to show any effect on asteroid shape brought on by planetary encounters.

TODO:

- acknowledgments
- justify throwing out the outliers
- MBA-equivalent comparison

Acknowledgments

Part I

Introduction

The study of the physical properties of asteroids is a key part of how we can understand the properties of the early solar system and how it formed. Asteroids represent a remnant of material left over from the early history of solar system formation that is largely unaffected by the various surface and internal processes that have altered the material that makes up the planets. However, that is not to say that the properties of asteroids have remained completely unchanged. Various gravitational and solar interactions experienced by asteroids have shaped the development of their properties over time (Bottke Jr et al., 2002). The diversity of asteroid properties and orbits and how they have changed make it so that an understanding of the asteroid population serves as a proxy for us to study the formation and evolution of the solar system.

Near-Earth objects (NEOs) are a particularly interesting subset of the asteroid population. Earth encounters in particular can be a major contributor to the development of these objects if their orbits allow them to have such encounters. These encounters are known to affect the properties of NEOs through tidal effects. Binzel et al. (2010) showed that weathered surfaces of asteroids are 'refreshed' upon an Earth encounter, causing less reddening to be observed than would otherwise be expected. Richardson et al. (1998) conducted numerical simulations which showed that the tidal forces encountered by Earth-crossing asteroids may cause mass shifting and removal during flybys, resulting in changes such as distortions, and formation of fragment trains and orbiting ejecta. Rotation on the asteroid Toutatis was studied by Takahashi et al. (2013), who showed that there was a significant shift in rotational angular momentum during periodic Earth flybys.

To study asteroid properties such as rotation and shape, photometric light curves are generated after a period of observation, from which these properties may be

extracted. A light curve is simply a plot of object magnitude over time. The magnitude seen in these light curves can vary due to changes in heliocentric and geocentric distance, rotation, and solar phase angle (Harris and Lupishko, 1989). The changes due to distance are generally removed during data reduction by using a 'reduced magnitude' value, but the periodic changes in brightness due to rotation and phase angle yield important information regarding the physical properties of the asteroid.

Rotational periods may tell us about the structure and collision history of an asteroid, while light curve amplitudes may tell us about the shapes of asteroids. Most larger asteroids (0.15 km $<$ D $<$ 10 km) are thought to be 'rubble piles' held together by self-gravity, since a spin rate barrier appears to exist, as larger asteroids are not observed to spin faster than this 'barrier' rate (Pravec et al., 2002). As spin states asymptotically approach rotation around the principal axis of maximum moment of inertia, asteroid light curves are expected to be at least double-peaked, with the exception of near-spherical or other degenerate cases. Light curve amplitudes are indicative of asteroid shapes because elongated asteroids may have greater variation between the least amount of light that it reflects and the most that it reflects.

This thesis expands on the studies done on asteroid-Earth encounters by building a method for automatic light curve fitting from magnitude data and by examining the effects of Earth encounters on asteroid rotational periods and amplitudes- values that may be obtained from light curves. An automatic light curve fitting routine was developed for the ongoing Mission-Accessible Near-Earth Object Survey (MANOS), which began in the latter half of 2013. However, due to the timing of MANOS, there is not enough data produced by the fitting routine to support a significant analysis of Earth encounter effects. As such, data from the Jet Propulsion Laboratory (JPL) and Minor Planet Center (MPC) were used in the analysis.

To approximate the probability of Earth encounters, the minimum orbit intersection distance (MOID) parameter was used. MOID is defined as the distance between the closest points of two bodies' osculating orbits. Here, MOID is a better param-

eter to use than the direct geometric distance between the Earth and the objects because the integration of an object's position in its orbit loses precision much faster than information about the orbit itself. This lends greater value to using MOID for timescales on the order of centuries or more. It is important to note, though, that MOID provides an estimate of the lower bound of the distance of an encounter. It does not guarantee that an encounter occurs, but simply suggests an increased likelihood with a lower value. Instantaneous MOID may be determined from the present-day orbital parameters of an object, and was used here to look at the relationship between encounters and period/amplitude.

Part II presents the background of NEO populations, the effects of planetary encounters on NEO rotational dynamics, and describes past and current asteroid surveys. Part III presents the automatic light curve fitting software developed as part of this project, particularly tailored for the ongoing nature and specific targets of MANOS. Part IV presents the results obtained from the Earth encounter analysis of this population of asteroids. Finally, Part V introduces future work that can be done to follow up on this project.

Part II

Background

1 The NEO Population

Asteroids, comets, and large meteoroids whose orbit intersects or nearly intersects Earth's are classified as Near-Earth Objects (NEOs). These objects are typically divided into three major categories based on their orbital elements: the Aten, Apollo, and Amor groups, which are collectively known as the AAA asteroids (Shoemaker et al., 1979). Atens are defined as objects having a semimajor axis $a < 1.0$ and an aphelion distance $Q \geq 0.983$ (the perihelion distance of Earth). This classification means that Aten objects only sometimes cross the orbit of Earth. Apollos are defined to have an $a \geq 1.0$ and a perihelion distance $q \leq 1.0167$ (the aphelion distance of Earth). Amors are defined solely by their perihelion distance, namely $1.1067 \leq q \leq 1.3$, meaning they are near-Earth-crossers but do not currently qualify as Earth-crossing asteroids. An NEO is considered a potentially hazardous object (PHO) if its minimum orbit intersection distance (MOID) is less than 0.05 astronomical units (AU) and has an absolute magnitude of 22.0 or less (JPL, 2014a). Orbital perturbations may, naturally, change the classification of any particular NEO between these groups.

The orbital characteristics of NEOs generally mean that they stay as NEOs for at most a few million years, eventually crashing into the Sun or terrestrial planets, or being flung out of the solar system (Binzel et al., 2002). The fact that the number of NEOs has remained steady over the last 3 billion years suggests that there is a source of resupply for the population (Bottke Jr et al., 2002). It is believed that main belt asteroids (MBAs) provide the bulk of NEO resupply, with Jupiter and Saturn resonances causing asteroids to move from main belt to NEO orbits. Smaller NEOs are likely collision fragments from MBAs, and exhibit younger (less-weathered)

surfaces due to the difficulty of surviving further collisions or planetary encounters (Binzel et al., 2002).

The NEO population is of special interest planetary astronomers because of its proximity to Earth. NEOs with low inclination and low eccentricity in particular are some of the best solar system targets for space missions due to the relatively low ΔV (a measure of the amount of effort required to change trajectories) and short time frame required to reach them. Additionally, the inner solar system orbits and periodic proximity to Earth of these NEOs mean that thermal and power considerations for rendezvous and flyby missions can be significantly simplified compared to near-Sun or outer solar system missions, making them relatively low-cost and within the reach of early private-sector space missions (Perozzi et al., 2001).

2 Planetary Encounters

Tidal forces encountered near the terrestrial planets cause a number of changes to asteroids. Distortion and disruption have been found to occur with Earth-crossing asteroids in numerical simulations, with results ranging from elongation and mass stripping, to the formation of fragment trains and binary systems. Low-inclination, low V_∞, and long-rotational-period asteroids experienced the most severe effects in these simulations (Richardson et al., 1998, Bottke Jr et al., 1998). Chapman (1978) argues that large, monolithic MBAs may have been fragmented by collisions to form rubble piles. The lack of observed fast-rotating asteroids with absolute magnitudes $H < 22$ suggests that larger NEOs are indeed such rubble piles and have minimal tensile strength, where any additional spin-up would cause disruption. Smaller NEOs, however, may remain monoliths due to the fact that they were spun off from these rubble piles. Fragment trains are generally formed from distortion processes that cause elongation, resulting in a pattern similar to what happened to Comet D/Shoemaker-Levy 9 during its 1992 Jupiter encounter (Shoemaker et al., 1979). Binary systems, on the other hand, are often formed from spin-up, which causes

rubble pile asteroids to fling mass off their equators, resulting in an orbiting body. The fact that about half of the observed fast-rotating ($P < 2.2\,h$) NEOs are binary systems supports the idea that Earth encounters cause strong enough disruptions to form binary systems (Pravec and Harris, 2000, Pravec et al., 2002, Walsh and Richardson, 2006).

Planetary encounters have also been shown to cause 'freshening' of the surface of asteroids. This process runs counter to the usual 'space weathering' process whereby asteroids become increasingly reddened. Binzel et al. (2010) showed that Mars and Earth-crossing asteroids that have closer encounters with the terrestrial planets tend to appear less weathered. This investigation involved using the Minimum Orbit Intersection Distance (MOID) parameter as a measure of the possibility of an Earth encounter, showing that for an integrated MOID, objects that likely had planetary encounters over the past 500,000 years showed less signs of weathering than objects that were kept away from a planetary encounter (perhaps by orbital resonance) (Binzel et al., 2010).

Numerical simulations across a distribution of asteroid spin states showed that while planetary encounters may cause either spin-up or spin-down or tumbling in individual asteroids, there is an overall trend towards spin-ups, one that is particularly prevalent for bodies with a slow initial rotation (Scheeres et al., 2004). Tumbling cases may be created only if the flyby occurs out of the asteroid's equatorial plane, as gravitational forces along the plane would at most cause a spin-up or spin-down (Scheeres et al., 2000).

Recently, radar imaging of 4179 Toutatis- an asteroid that makes periodic near-Earth flybys- gave a series of observations that showed terrestrial tidal torques altering the rotational dynamics of the asteroid. These torques mostly caused changes in orientation as the asteroid passed close to the Earth, but a particularly close encounter in 2004 demonstrated a significant perturbation in the angular momentum of the asteroid that persists to the present (Takahashi et al., 2013).

3 Asteroid Surveys

New technologies have shifted the observing focus from larger, multi-kilometer-sized MBAs and NEOs to smaller sub-kilometer-sized NEOs. Asteroid surveys in the past have been able to find and characterize thousands of main-belt and near-Earth asteroids. Many past surveys focused on discovery, with examples including LONEOS, LINEAR, Catalina, and Pan-STARRS. Some studies were specifically for characterization of known objects, such as the albedo characterization done by IRAS, WISE and Akari, and the spectral characterization done by SMASS. These surveys were able to extensively sample the population of asteroids that is larger than the rubble pile limit; however technological limitations meant that they were biased towards being able to observe larger, brighter objects, rarely being able to resolve asteroids dimmer than 22nd absolute magnitude (Binzel et al., 1989, Jedicke et al., 2002, Stokes et al., 2002).

The past decade has seen a rapid increase in the number of NEO detections, partly due to advances in observation and computing technologies, but also because of increased urgency started by a mandate by the American government to characterize 90% of NEOs larger than 1 km that may present an impact hazard to Earth (Binzel et al., 2002). A new, multi-year program started in August of 2013 called the Mission Accessible Near-Earth Object Survey (MANOS) seeks to leverage advances in observing capabilities to characterize asteroid targets that are more than an order of magnitude smaller than those covered by previous studies. Using telescopes such as Gemini, SOAR, Kitt Peak 4m, and CTIO, MANOS is specifically focusing on sub-kilometer-sized targets that would be accessible by space missions utilizing conventional chemical propulsion, providing rough characterization of targeted NEOs via astrometry, light curves, and spectra. Mission-accessible is defined to be having a $\Delta V < 7$ km/s, which is the approximate limit of conventional chemical propulsion. The program aims to characterize approximately 100 NEOs per year, meaning that there will be a large throughput of data during the survey period, which is expected

to last 3 to 5 years. This thesis draws much of its data from the MANOS dataset, and a part of the work done for the thesis was development of automated data processing software for the MANOS pipeline.

TODO - how to cite MANOS info

Part III

Light Curve Fitting

In order to automate part of the data processing done on incoming MANOS data, a fitting routine, manosCurveFit, was developed by the author to automatically scan reduced MANOS photometry data and convert them into a light curve model which provides the period and amplitude. Before this work, curve fitting for MANOS was done using software built on MATLAB, which contained some components that were relatively poorly documented and required a proprietary platform. Other common fitting methods, such as Canopus, were similarly based on proprietary software. manosCurveFit was developed from scratch specifically for the MANOS data pipeline and represents one of very few pieces of light curve fitting software that is free and open source, and possibly the only such software that is tailored for asteroid fits.

1 Software Details

1.1 System Overview

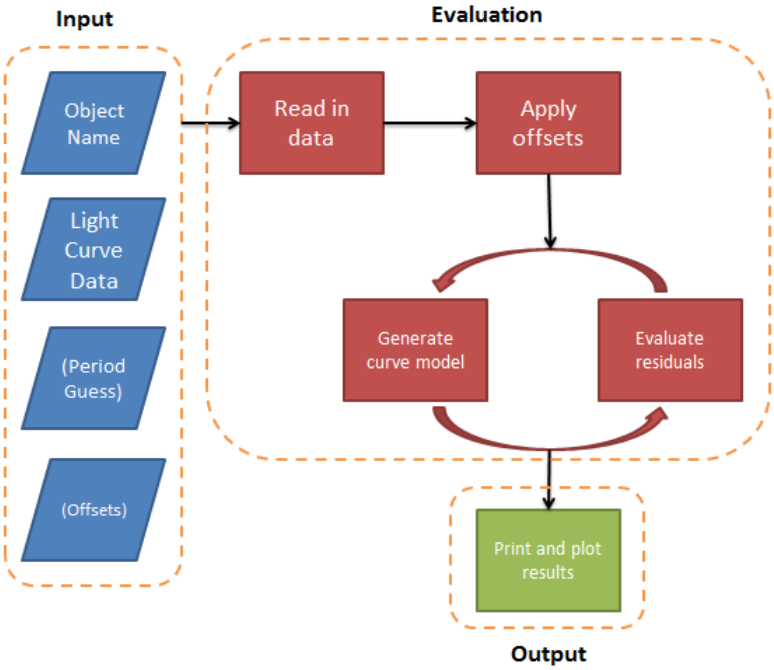

Figure 1: Flowchart showing the conversion from raw data to fitted plots. The dashed boxes represent the three main parts of the software.

The fitting routine fits a mathematical model to light curve data. The fitting process may be generally divided into input, evaluation, and output portions. The inputs in parentheses are not required for the fitting to work, but a guess at the rotational period may significantly constrain the search space, and if data is taken over multiple nights and/or by different instruments, offsets are required to normalize the magnitudes to some baseline. A number of other inputs may also be supplied to constrain or expand the search space. These inputs may be supplied by the fitInfo file for each object. The light curve data is then read in from one or more text files with standardized columns.

Two kinds of magnitude offsets are then applied: offsets by night/instrument, if provided, and a normalizing offset which subtracts the weighted average magnitude of the set from the entire set. The normalizing offset is necessary in order to center

the data points on the y-axis for fitting purposes, and may be used in this context because only differential magnitudes are needed. This acts as a coarse adjustment for y-axis centering. A finer adjustment is made by a y-axis offset for the model, which is taken to be part of the least squares minimization. For each period to be checked, a least squares minimization is performed for each order of Fourier coefficients from two to six, unless specified otherwise in the fitInfo file. The parameters that generate the best fit to the data are kept and printed at the end, along with the light curve and residual plots.

See the Appendix for further software documentation.

2 Fitting Rationale

This fitting routine is based on equations 1, 2, and 3 from Harris and Lupishko (1989) (corresponding to equations 1, 3, and 4, below), which describe the fitting model for a light curve, the residuals of the model, and the bias-corrected variance, respectively. The fitting model is described by the Fourier Series

$$H(\alpha,t) = \bar{H}(\alpha) + \sum_{L=1}^{m} A_L sin\frac{2\pi L}{P}(t-t_0) + B_L cos\frac{2\pi L}{P}(t-t_0). \quad (1)$$

$\bar{H}$ is a correction to get the absolute magnitude of the asteroid. Absolute magnitude is defined to be the visual magnitude of an asteroid if it were at zero phase angle and at 1 AU from both the Earth and the Sun, which, in combination, is actually a set of unphysical conditions (JPL, 2014b). Here, $\bar{H} = 0$ because absolute magnitudes are not necessary for MANOS, and m (the series order), P (the period), and A_L and B_L (the Fourier coefficients) are free parameters. Since a fine-adjustment y-shift is also added, the actual fitting equation becomes

$$H(\alpha,t) = y + \sum_{L=1}^{m} A_L sin\frac{2\pi L}{P}(t-t_0) + B_L cos\frac{2\pi L}{P}(t-t_0), \quad (2)$$

where y is an additional free parameter, which generally takes on a small value.

The residual of a particular observation i may be obtained by

$$\frac{\delta_i}{\epsilon_i} = \frac{V_i(\alpha_j) - H(\alpha_j, t_i)}{\epsilon_i}, \tag{3}$$

where α_j is the reference phase angle on the j^{th} night, t_i is the time of the i^{th} observation, and ϵ_i is the error of the measurement. In the context of NEOs, the phase angle may very well change, particularly as targets pass very close to Earth. However, the majority of MANOS targets will be observed for a short period of time (on the order of a few hours) and characterization of these targets will be done solely on the basis of a one-time observation. Therefore, α will be assumed to be a constant due to the time scales involved in the single observation, and as such, manosCurveFit does not take phase angles into account. The least squares minimization is then performed on the bias-corrected variance, given by

$$s^2 = \frac{1}{n-k} \sum_{i=1}^{n} \left(\frac{\delta_i}{\epsilon_i} \right)^2 = minimum, \tag{4}$$

where n is the total number of observations, $k = 2m + 1$, where m is defined in 1. The total number of nights of data is also added into k in the form that Harris et al. use, but here, this again needs not be considered because we are concerned with differential photometry, and offsets for different nights will be provided as necessary.

By default, the program will run the fit from $m = 2$ to $m = 6$. The minimum of order two is due to the fact that asteroid light curves are expected to be double-peaked (except for some cases of complex rotation or degenerate cases of near-spherical bodies), and the maximum of order six is used to prevent over-fitting. The curve is centered around zero magnitude by a weighted average of the data, but since there is often still a slight magnitude offset due to the nonuniform nature of the sampling, a magnitude offset parameter was added to allow for a better fit. The user does not normally interact with the optimization of this y-shift parameter.

Precautions were taken to prevent over fitted or unsubstantiated models. Any

models which produce amplitudes greater than 2 are rejected. This is necessary to prevent the fit from assuming a model in which the data are a small portion of a much longer period with one or more large spikes where data is not present. As an additional precaution, if the fitted period is more than 25% of the range of the phase-folded data points, a warning is given to notify the user of a potentially under-constrained model.

3 Fitting Results and Data Products

By default, the software automatically produces two figures and a text file report of the fit, which are then saved to the same folder as the data. Examples of these for plots may be seen in Figures 2 and 3. The bottom sub-plot of Figure 2 is an optional plot which shows the residuals of the generated fit. This plot may be used as an additional manual check on the fit by seeing if any structure or bias remains in the residuals, which may indicate that a higher-order fit is required. Additionally, any significant magnitude bias in the residuals plot may indicative of an incorrect offset of a particular night, if multiple nights' data are used (this effect should also be viable in the main fitted plot). Figure 3 shows the RMS values of different periods that were attempted during the fitting process, with the fit that provided the minimum RMS value representing the fit that was eventually accepted. These figures represent a set of data that was composed of 12 nights, split into two input text files, all of which were automatically merged and processed by the program. This kind of dataset is more complex than most typical MANOS datasets, which will generally be data from a few hours on one instrument for a single night, so multiple input files and automatic merging will largely be unnecessary.

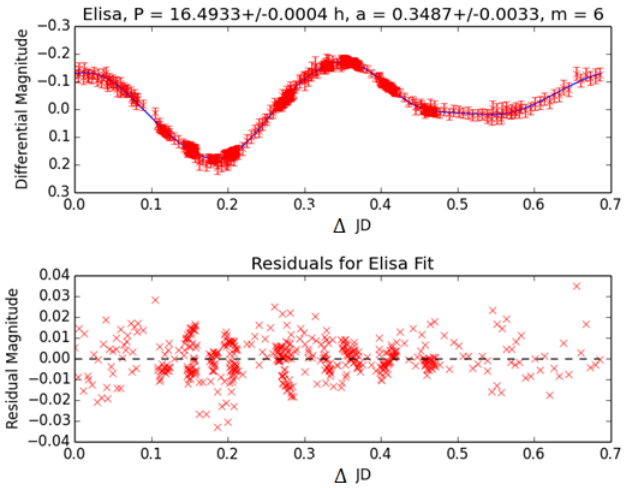

Figure 2: One of the figures produced by manosCurveFit, showing the data points on top of the fitted model (top) along with the residuals of the fit (bottom). The model automatically phase-folded the data to give the best fit, and the residuals here show an example of what would occur for a good fit, since there is no notable bias or structure in the residual plot. The residuals plot shows a line at zero magnitude to help in finding any structure or bias.

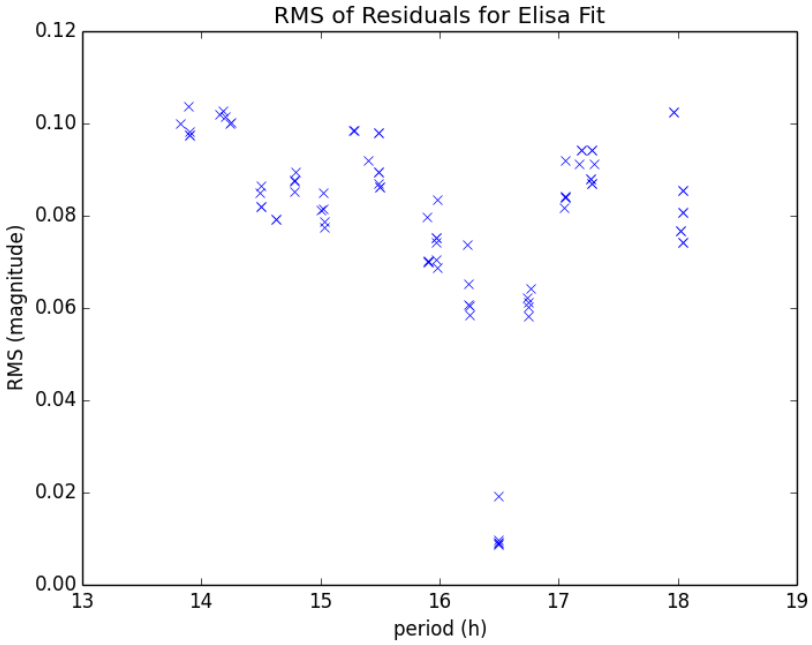

Figure 3: The second figure produced by manosCurveFit, showing the mean RMS values of the fit when different periods are attempted.

The fitting routine was tested against five objects with varying light curve structures, three of which had previously-determined periods. Table 1 shows the compar-

ison between the fitted and accepted periods of the latter three objects, all of which showed very low error values (if any), even though the data used for the fit is only a small subset of the entire set of data used to generate the accepted period. 2579 Spartacus had a different fitted period than accepted period likely due to the fact that the accepted period is based on a much larger baseline of data than what was used for the fit.

Table 1: Period comparisons between fit and accepted values.

Object	**Fitted Period (h)**	**Accepted Period (h)**	**Error**
2012 DA_{14}	5.95 ± 0.12	5.8 ± 0.3	consistent
956 Elisa	16.4933 ± 0.0004	16.494 ± 0.001	consistent
2579 Spartacus	3.812 ± 0.019	3.63599 ± 0.00004	4.84%

Part IV

Analysis of Physical Properties with Respect to Earth Encounters

1 Overview and Hypothesis

NEO light curve frequencies, light curve amplitudes, and absolute magnitudes were compared to their MOID values. Data analysis sought to find differences in the distribution of these values over selected subsets, leveraging the aggregated values of groups of NEOs to look for trends in the overall data. Since MOID presents only a lower bound of the actual intersection distance, a small MOID does not guarantee that an object actually passed near the Earth, but rather only increases the likelihood that it did. A trend in the properties of the distribution within these groupings with respect to MOID would be a possible indicator an Earth encounter effect. The focus of the comparison is between objects that may have had an Earth encounter, and those that have not. A rough boundary for a MOID that is indicative of a possible Earth encounter is a value of $<$0.0026 AU, or $<$1 lunar distance (LD). Thus, this boundary was used to separate the asteroid population into two groups: a $<$ 1 LD group that may have had an Earth encounter, and a $>$ 1 LD group that is extremely unlikely to have had an Earth encounter.

Based on the literature review presented in Section 2- particularly the simulations of Earth encounters done in Scheeres et al. 2000 and Scheeres et al. 2004- it is hypothesized that a population of objects that have undergone a planetary encounter will likely have greater variation in rotational period and amplitude. This variation is, however, unlikely to be very pronounced, as the limitations of MOID mean populations with some, but not all, objects that have had some Earth encounter is the best that can be selected. Again noting the simulations done by Scheeres et al. (2004), it

is hypothesized that the analysis may show a slight spin-up in objects that have had planetary encounters, but this again will likely prove difficult to show (perhaps only showing possible statistical significance in some cases, and no statistical significance) because the simulations showed that spin-up is a prominent effect only in asteroids with initially slow rotations, which cannot be distinguished in the data being used.

TODO - MBA-equivalent comparison?

2 Data Analysis Method

2.1 Description of NEO Data

Two main sources of data were polled for the analysis done in this project. The Jet Propulsion Laboratory's (JPL) Horizons database was polled for MOID, magnitude, and rotational period (but did not contain light curve amplitude information). Two databases were taken from the Minor Planet Center (MPC)- one of light curve and one of NEOs- and combined to obtain MOID, magnitude, rotational period, and amplitude information. The MOID values from both sources were instantaneous MOIDs calculated from the present-day orbital elements. The Horizons dataset contained 10938 objects, 10775 of which contained both magnitude and MOID information, 685 of which contained both rotational period and MOID information, and 680 of which contained all three. The analysis done for rotational frequency was done using the Horizons data.

The MPC's NEO datasets contained information for 827 Aten, 5306 Apollo, and 4500 Amor objects when it was polled for this project in March of 2014, while the light curve database contained 2326 objects. The light curve database had the amplitude and period information for each object, but lacked MOID data, which was contained in the NEO dataset. As such, it was necessary to merge the two sets, cross-referencing objects contained in both to obtain a complete listing of light curve properties and MOID. The resulting set contained 274 objects, of which 245 contained

amplitude, magnitude, and MOID information. Since this dataset contained light curve amplitude values, it was used for the amplitude analysis.

3 Results

3.1 Magnitude

The absolute magnitude (H) was plotted against the MOID of the objects. On the semi-log plot shown in Figure 4, it can be seen that objects with higher H values tend to have lower MOIDs, which fits with the observational bias of being more likely to see dimmer objects if they pass closer to Earth.

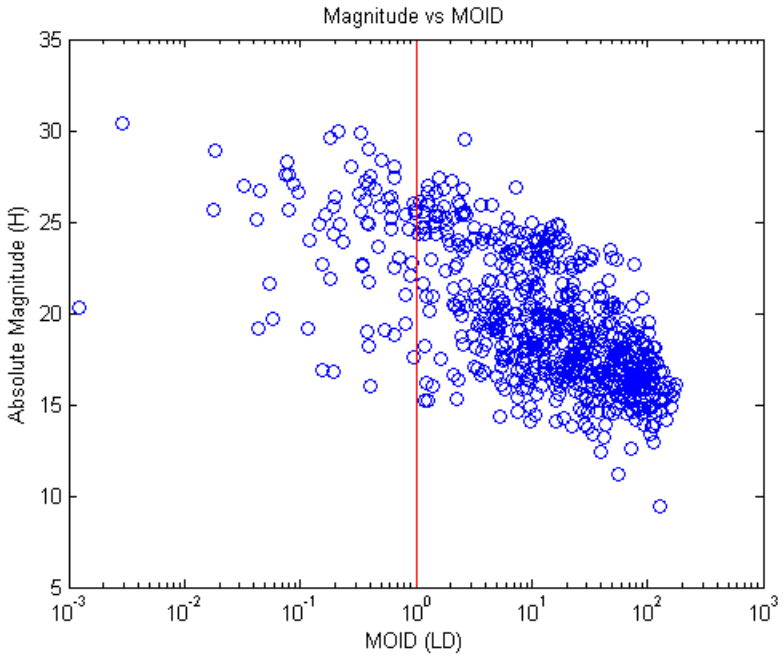

Figure 4: Semi-log scatterplot of absolute magnitude against MOID value shows a correlation where dimmer (smaller) objects tend to have lower MOID values. The red line represents 1 LD.

3.2 Rotation Frequency

As an initial examination of various possible effects on rotation frequency, frequency was plotted against MOID (Figure 5) and absolute magnitude (Figure 6).

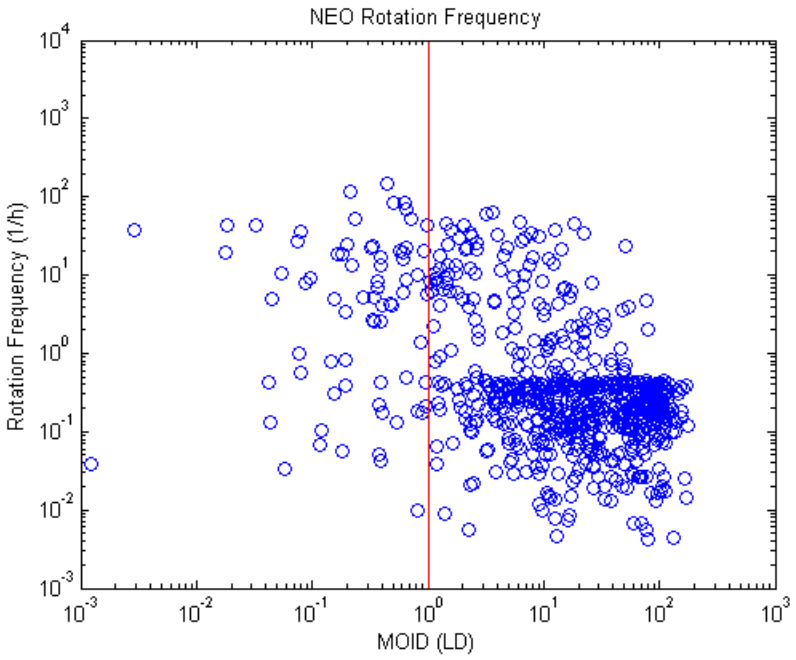

Figure 5: Frequency vs. minimum orbit intersection distance for Aten, Apollo, and Amor (AAA) NEOs.

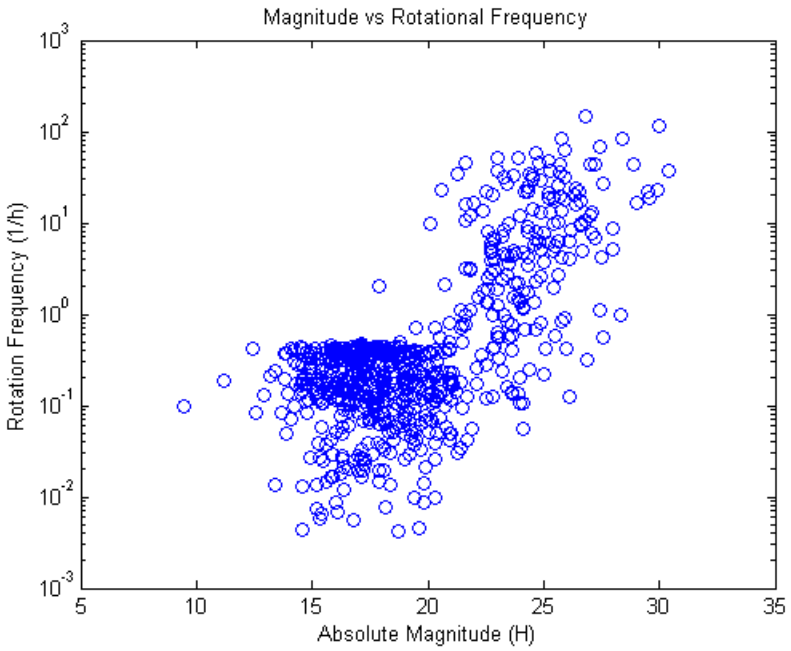

Figure 6: Plot of absolute magnitude against rotational frequency. Higher-magnitude (smaller) objects tend to have faster rotations.

A 30-window moving average plot was then used to examine the mean and standard deviation of frequency as a function of MOID, as shown in Figure 7. It should be noted that for moving average plots such as this, consecutive mean and standard deviation values are not independent, and independence of these values only occurs for points that are at least one window apart (i.e. points that have at least 30 other points between them).

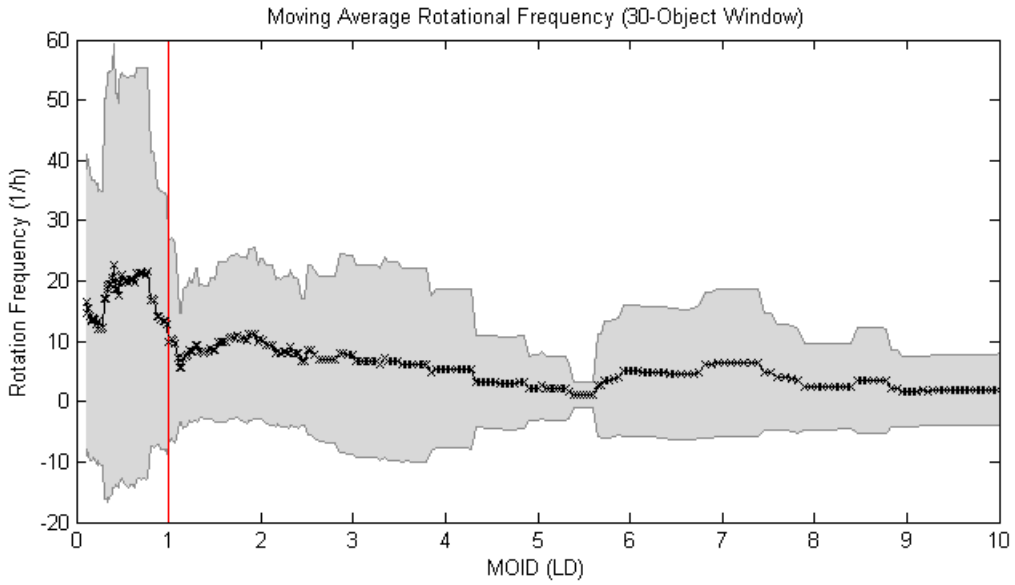

Figure 7: Moving average plot of rotational frequency (without bias correction) with a 1-LD reference line. Each 'x' mark represents the mean MOID of one 30-object window, and the shaded region represents one standard deviation of the mean above and below the mean value.

However, it may be seen from Figure 6 that objects that have higher magnitudes (likely to be smaller objects) tend to display faster rotations, which is consistent with the asteroid collision evolution model predicted by Chapman (1978). This makes the result given by Figure 7 less reliable, since it is likely to be biased by the fact that dimmer asteroids are more likely to be observed closer to Earth (Figure 4), and these dimmer asteroids are likely to be smaller and therefore have higher rotational frequencies (Figure 6). In order to better examine the distribution of rotation frequencies as a function of MOID, a correction must be made for this size/rotation bias. Thus, when analyzing the frequency distributions, only objects within a certain range of magnitudes were compared to each other. Figure 8 shows two selected populations based on absolute magnitude.

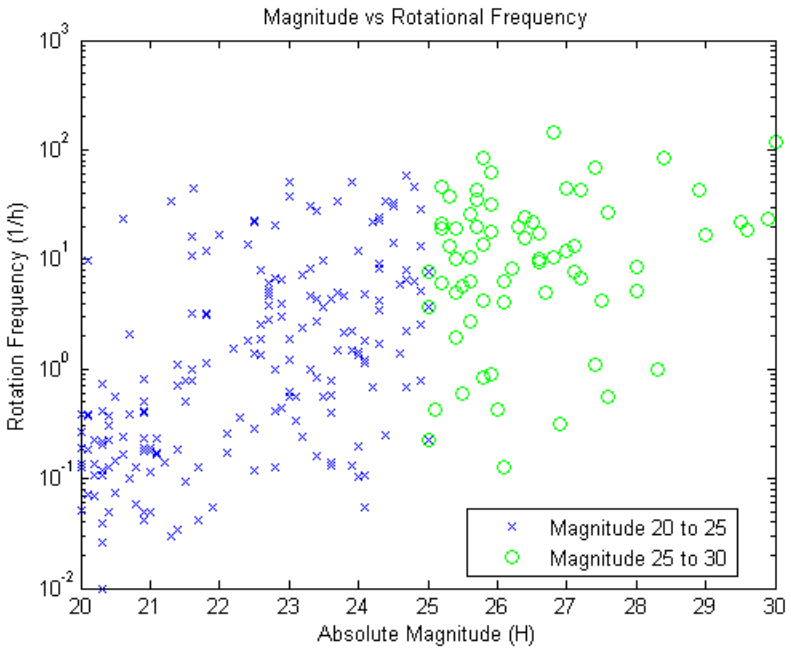

Figure 8: Plot of absolute magnitude against rotational frequency for objects of magnitude 20 to 30. These magnitude ranges were chosen due to the number of objects and the range of rotational frequencies represented in them. The general bias towards larger objects having lower frequencies should largely be removed within independent examinations of each of these two populations.

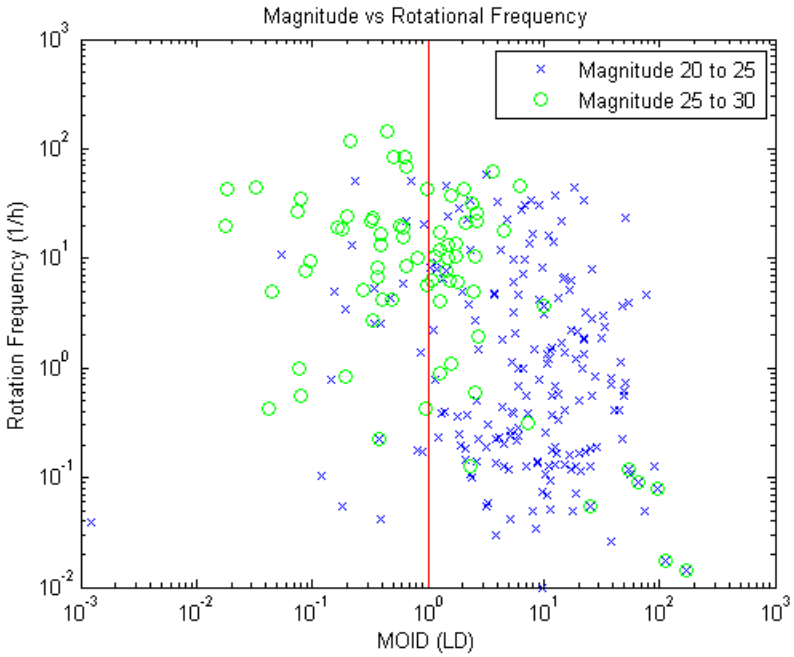

Figure 9: Comparison of the MOID vs rotational frequency distribution for objects ranging from magnitude 20 to 25, and 25 to 30. The sample size of objects in the 25 to 30 magnitude range becomes much smaller past a few lunar distances.

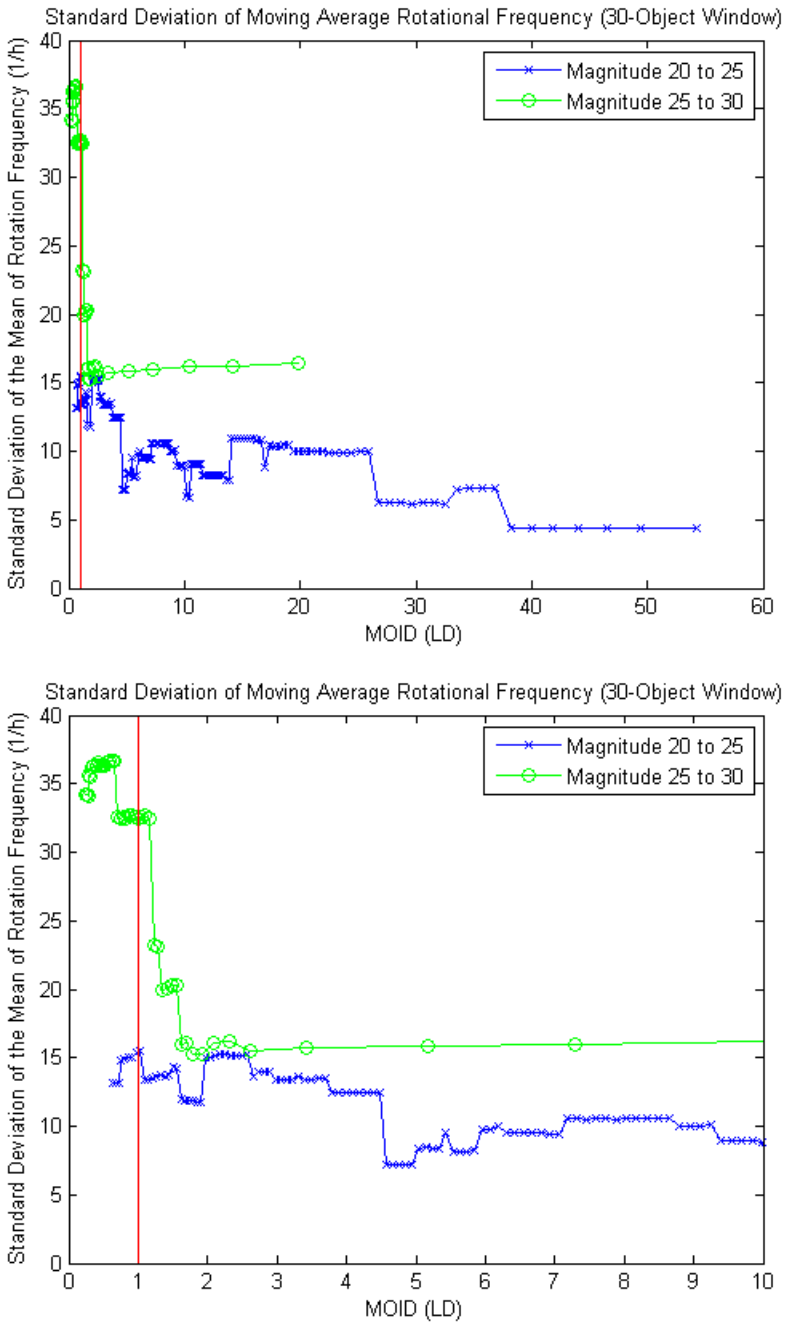

Figure 10: Plot of standard deviation of the mean of 30-object samples of objects in the magnitude range from 20 to 25. 1-LD line inserted for reference. The plot on the bottom is a zoomed in (0 to 10 LD) version of the plot on the top.

A two-sample one-tailed Student's t-test was conducted to see if there was a statistically significant difference between the means of the rotational frequencies of objects in the MOID range where planetary encounters are possible and other MOID ranges, specifically if the frequencies in the group that had smaller MOID values were

greater than the frequencies of the group with larger MOID values. Similarly, a two-sample one-tailed f-test was conducted to see if there was a statistically significant variance between the rotation frequencies of different populations, specifically if the variance of the frequencies in the group that had smaller MOID values was greater than the variance seen in the group with larger MOID values. The two samples for each test were binned according to a dividing MOID value, for which one sample ranges from 0 to the dividing MOID, and the other ranges from the dividing MOID to the maximum MOID value in the data set (174 LD). Dividing MOID values were chosen to range from 1 to 10 LD, since objects crossing within 1 LD are likely to have experienced some encounter effect, and the inverse square drop-off of gravity means that at 10 LD, the effect of gravity is one one-hundredth of its effect at 1 LD, meaning all asteroids with some planetary encounter effect should have been captured in the first bin by the time the dividing MOID is at 10 LD. The sizes of the groupings are shown in Tables 2 and 3 where 174 LD represents the MOID of the furthest object in the dataset. The results of the t-tests and f-tests are shown in Figures 11 and 12, where p values lower than 0.1, 0.05, and 0.01 represent possibly significant, significant, and highly significant differences between the two samples.

TODO - is this binning explanation clear enough?

Table 2: Number of objects in the closer (n_1) and further (n_2) MOID groups for objects of 20th to 25th magnitude used for frequency analysis..

n_1**range (LD)**	n_1	n_2 **range (LD)**	n_2
0 to 1	22	1 to 174	177
0 to 2	39	2 to 174	160
0 to 3	53	3 to 174	146
0 to 4	64	4 to 174	135
0 to 5	72	5 to 174	127
0 to 6	84	6 to 174	115
0 to 7	94	7 to 174	105
0 to 8	99	8 to 174	100
0 to 9	104	9 to 174	95
0 to 10	111	10 to 174	88

Table 3: Number of objects in the closer (n_1) and further (n_2) MOID groups for objects of 25th to 30th magnitude used for frequency analysis.

n_1**range (LD)**	n_1	n_2 **range (LD)**	n_2
0 to 1	39	1 to 174	37
0 to 2	54	2 to 174	22
0 to 3	64	3 to 174	12
0 to 4	65	4 to 174	11
0 to 5	66	5 to 174	10
0 to 6	66	6 to 174	10
0 to 7	67	7 to 174	9
0 to 8	68	8 to 174	8
0 to 9	68	9 to 174	8
0 to 10	68	10 to 174	8

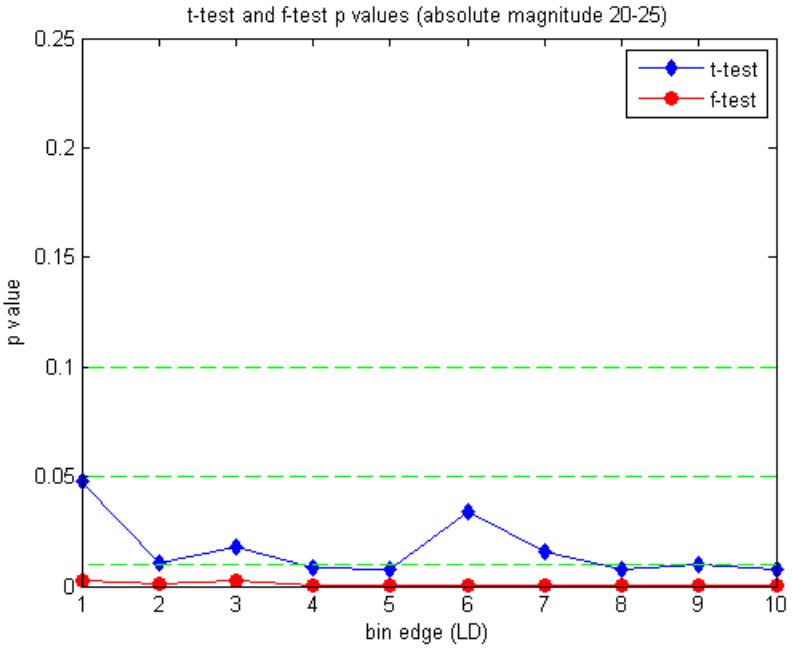

Figure 11: Results of one-tailed Student's t-tests, and one-tailed f-tests conducted for objects of 20th to 25th magnitude. Dashed lines represent p values of 0.1, 0.05, and 0.01, respectively.

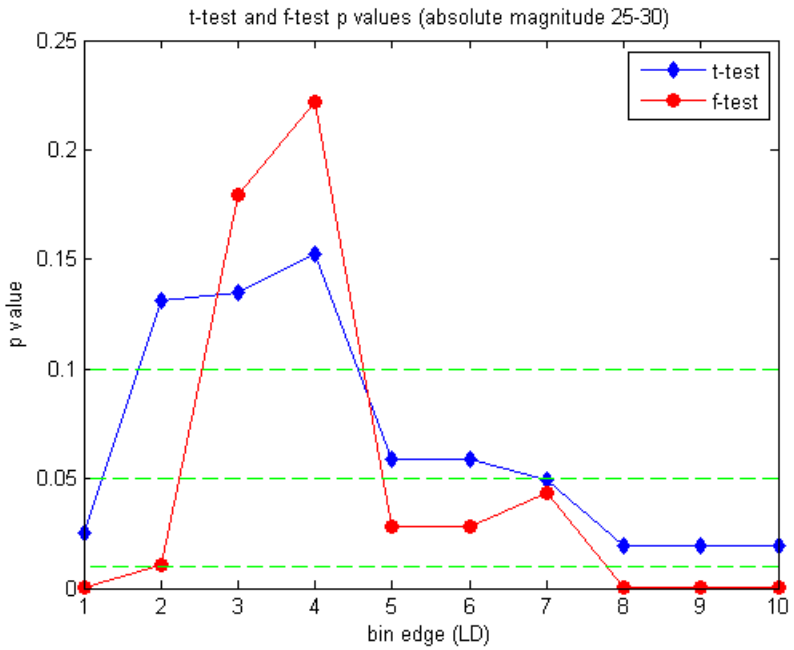

Figure 12: Results of one-tailed Student's t-tests, and one-tailed f-tests conducted for rotation frequencies of objects of 25th to 30th magnitude. Dashed lines represent p values of 0.1, 0.5, and 0.01, respectively.

3.3 Amplitude

Light curve amplitude was also examined as an asteroid property using a procedure similar to the one done for rotational frequency. When examining a light curve, the amplitude is the difference in magnitude between the maximum observed brightness and the minimum observed brightness in curve. Amplitude is indicative of asteroid shape, since elongated shapes will produce larger variations in brightness when spinning along a principal axis of maximum moment of inertia. In these cases, the objects will be brighter to an observer when their elongated side is reflecting the most light towards Earth, and dimmest when their shorter sides are reflecting the most light. There may be, of course, cases of elongated asteroids spinning along their long axes, but these cases are unlikely due to the tendency of spin states to evolve towards axes of maximum moments of inertia due to their lower energy states.

Amplitude bias correction was performed using the procedure described in Binzel and Sauter (1992). This procedure was used to correct for a bias introduced by

possible under sampling of light curves, which would generate a lower estimate of the amplitude. The procedure attempts to bring the amplitude estimate as close as possible to what it would be if the object was observed at a 60° phase angle.

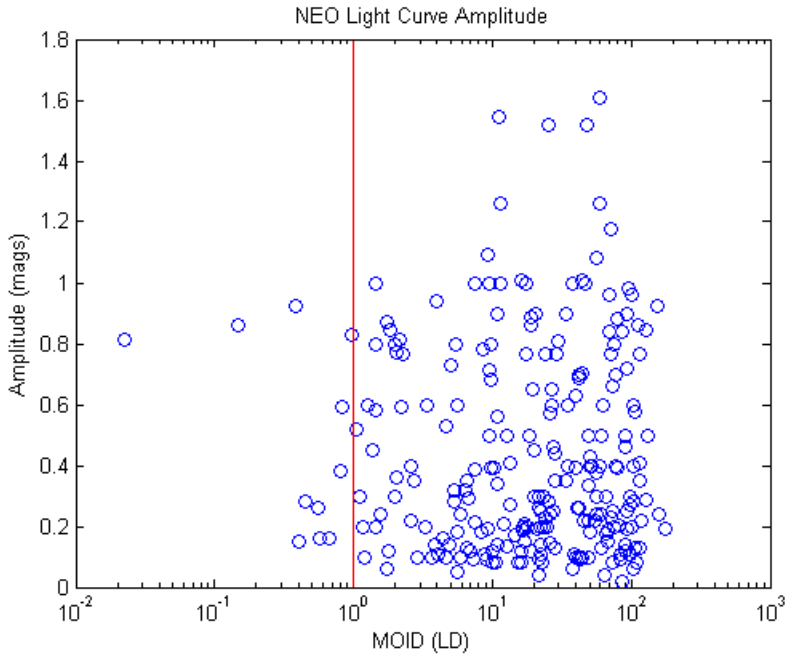

Figure 13: Bias-corrected amplitude vs. minimum orbit intersection distance for Aten, Apollo, and Amor (AAA) NEOs. The red line represents 1 LD.

Again, the property being examined was plotted against the object magnitude to check for correlation to see if the population needed to be subdivided to eliminate a magnitude bias. In this case, however, it may be seen in Figure 14 that such a correlation does not exist for amplitude, so the kind of de-biasing used for rotational frequency is not needed.

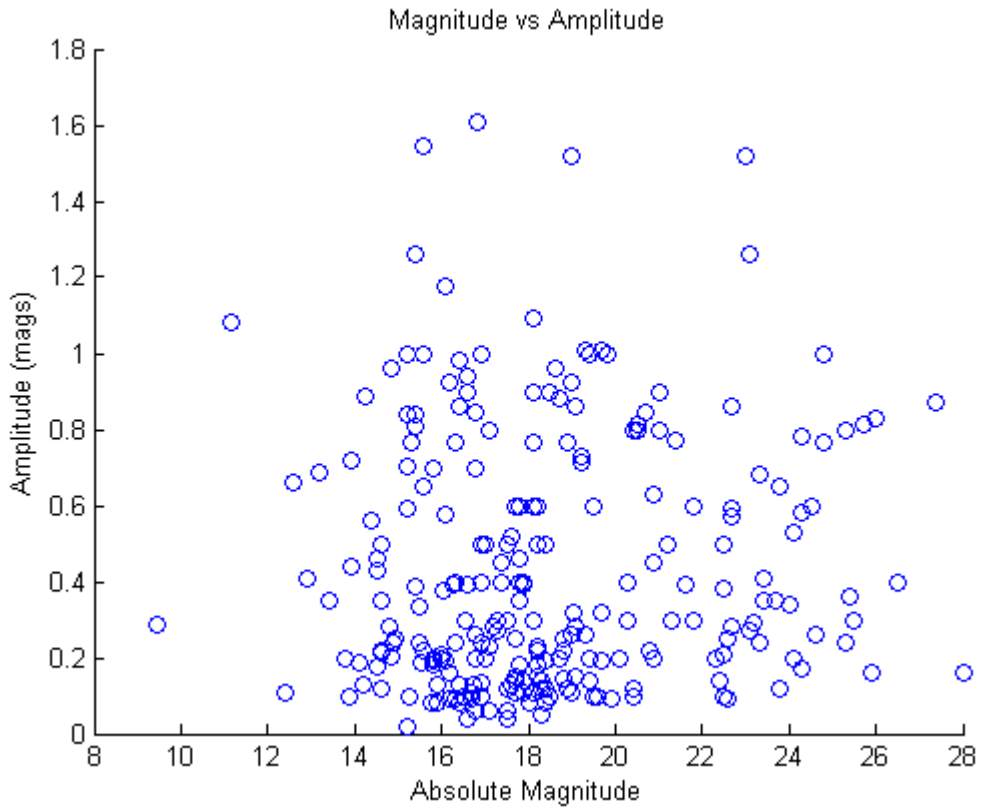

Figure 14: Plot of absolute magnitude against the light curve amplitude. In contrast to Figure 6, no noticeable correlation exists between absolute magnitude and light curve amplitude.

Next, a 30-object moving window average was applied to this sample, as shown in Figure 15. The standard deviations produced by this moving window procedure are shown in Figure 16. From these plots, it can be seen that the standard deviation is large compared to the change in the mean amplitude, and the mean amplitude never moves beyond the error bars.

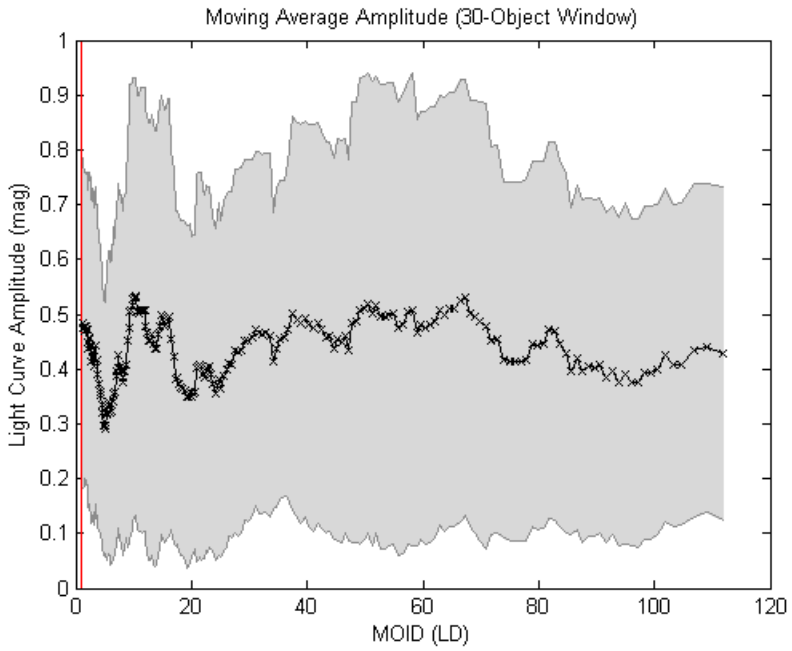

Figure 15: Moving average plot of light curve amplitude with a 1-LD reference line. Each 'x' mark represents the mean MOID of one 30-object window, and the shaded region represents one standard deviation of the mean above and below the mean value.

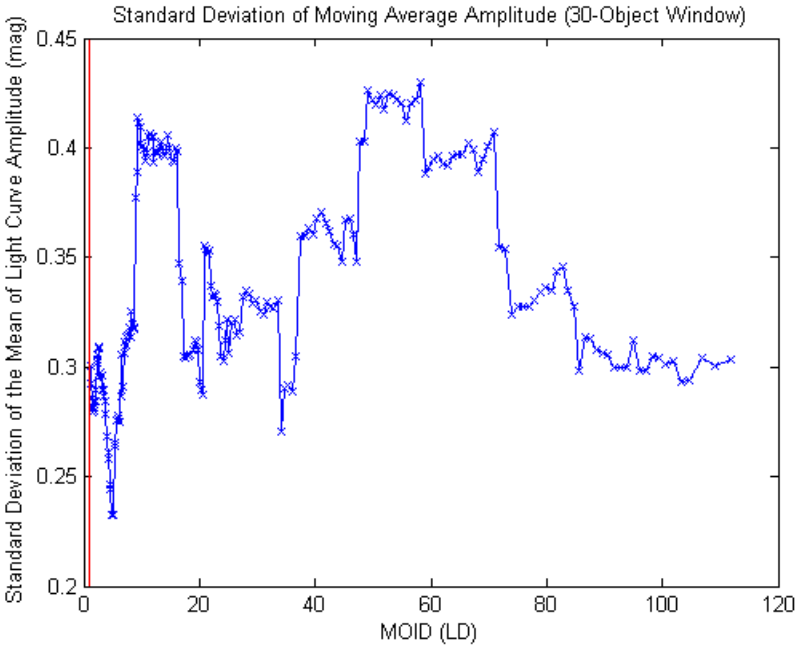

Figure 16: Plot of standard deviation of the mean of 30-object samples of objects in the magnitude range from 20 to 25. 1-LD line inserted for reference.

Finally, a two-sample one-tailed t and f-tests were conducted, using a MOID value ranging from 1 to 10 LD as the dividing value between the two samples. The sample ranging from 0 LD to the dividing MOID represent the population that is more likely to have experienced an Earth encounter, and the sample from the dividing value to 174 LD represents a population that is likely to not have experienced such an encounter. The p values produced by these tests may be seen in Figure 17.

Table 4: Number of objects in the closer (n_1) and further (n_2) MOID groups use for amplitude analysis.

n_1**range (LD)**	n_1	n_2 **range (LD)**	n_2
0 to 1	11	1 to 174	235
0 to 2	27	2 to 174	219
0 to 3	37	3 to 174	209
0 to 4	43	4 to 174	203
0 to 5	48	5 to 174	198
0 to 6	57	6 to 174	189
0 to 7	62	7 to 174	184
0 to 8	66	8 to 174	180
0 to 9	69	9 to 174	177
0 to 10	79	10 to 174	167

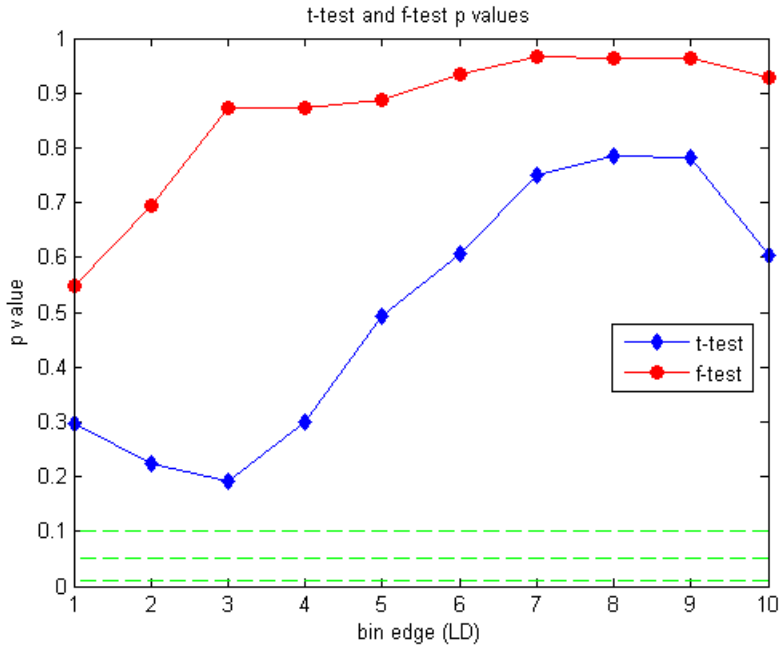

Figure 17: Results of one-tailed Student's t-tests, and one-tailed f-tests conducted for light curve amplitudes. Dashed lines represent p values of 0.1, 0.5, and 0.01, respectively.

These statistical tests show that the data do support the idea that near-Earth encounters significantly affect the shapes of NEOs.

4 Discussion

4.1 Rotational Frequency

From Figure 11, it can be seen that from the sample of objects that range from 20th to 25th magnitude, results of all the f-tests for pairs of samples divided by MOID values ranging from 1 to 10 LD all show a highly statistically significant difference in variance, indicating that populations of objects that have had a planetary encounter have a higher variance in rotational frequencies than those that did not. Similarly, all of the t-tests return significant or highly significant differences, indicating that the set of objects with lower MOID had higher rotational frequencies than the set with lower MOID.

In the sample of objects that range from 25th to 30th magnitude, the majority of results from both t and f-tests return some statistical significance, there is a noticeable jump in p values for both tests when the bin division line is between 2 and 5 LD. However, the quality of these results is rather low once the dividing point is past 2 LD, since the number of objects in the further bin drops significantly, as can be seen in Table 3.

The larger sample size and range of MOIDs present in the 20-25th magnitude group makes it a more reliable group for statistical testing. With the brightness (size) to spin rate bias largely removed by restricting the samples to a small magnitude range in both cases, these results confirm the hypothesis that populations which experience near-Earth encounters see both a increased variation in rotational frequency, as well as an overall increase in the frequencies. The statistical tests returned more significant results than were predicted on both counts.

4.2 Light Curve Amplitude

The data do not support the hypothesis that light curve amplitude is affected by near-Earth encounters. As noted in the hypothesis, this is a particularly difficult phenomenon to show, since the effect only occurs with very close encounters and/or larger rubble piles. Table 4 shows that the number of objects in the 0 to 2 LD MOID range is actually smaller than the typical minimum sample size of 30 for statistical analysis, which means that there simply is not enough information on low-MOID objects to conduct a proper analysis in the region where the amplitude effect is expected to be most easily observable. Supplementing the existing data with incoming MANOS data would likely improve the situation, but is outside the scope of this project.

Part V

Future Work

1 Light Curve Fitting

A number of improvements have been identified for manosCurveFit, largely to expand the kinds of inputs that the program can take, and partly to improve the fitting routine directly. Currently, the inputs for manosCurveFit can only be floats. It would be useful to expand the inputs to include strings, as many data files use strings to represent properties such as filter types and instruments, which currently are not accounted for in the data that is read into the program. Another improvement involves cases when data from multiple nights or telescopes are used. In these cases, an offset must be provided to each night except for one to bring all the magnitudes to the same baseline. However, in some cases, it would be easier to leave the offsets as a free parameter that can be optimized for in the same way as the other free parameters, which eliminates the need to estimate the offsets.

Finally, to account for cases when multiple nights' data are used in which the nights are spread further apart (currently not the case with MANOS), phase angle considerations may be added to the fitting routine. To do this, orbital parameters must be known for the objects being analyzed. Since the fitting code is primarily operated on computers at Lowell Observatory, it would make sense to have it poll Lowell's databases for orbital parameters once the proper infrastructure is in place for such a system.

2 Data Analysis

Additional analysis can be done to improve the work done in this project. As previously mentioned, the dataset could be supplemented by MANOS, which would fill

in gaps in the data, particularly on high-magnitude, close-range objects. Integrated MOID would also likely prove to be a useful way to look at the data. Integrated MOID provides a more accurate picture of the likelihood of planetary encounters by integrating the orbit of an object (along with a number of virtual clones of the object offset by some distance) back in time, generally providing lower MOID bounds than an instantaneous calculation from present-day parameters would give. This method was used by Binzel et al. (2010) to show the asteroid 'freshening' effect of near-Earth encounters, and would likely prove useful here as well. Finally, as a comparison to a population of asteroids for which planetary encounters are even less likely than high-MOID NEOs, populations that are likely to have had encounters could be compared to main belt equivalent asteroids. In this case, NEOs could be grouped by absolute magnitude and compared to main belt asteroids of similar magnitudes to see the difference when compared to a more 'pristine' sample.

References

Richard P Binzel and Linda M Sauter. Trojan, hilda, and cybele asteroids: New lightcurve observations and analysis. *Icarus*, 95(2):222–238, 1992.

Richard P Binzel, Paolo Farinella, Vincenzo Zappala, and Alberto Cellino. Asteroid rotation rates-distributions and statistics. In *Asteroids II*, volume 1, pages 416–441, 1989.

Richard P Binzel, Dmitrij F Lupishko, Mario Di Martino, Richard J Whiteley, and Gerhard J Hahn. Physical properties of near-earth objects. *Asteroids III*, 255, 2002.

Richard P Binzel, Alessandro Morbidelli, Sihane Merouane, Francesca E DeMeo, Mirel Birlan, Pierre Vernazza, Cristina A Thomas, Andrew S Rivkin, Schelte J Bus, and Alan T Tokunaga. Earth encounters as the origin of fresh surfaces on near-earth asteroids. *Nature*, 463(7279):331–334, 2010.

William F Bottke Jr, Derek C Richardson, and Stanley G Love. Production of tunguska-sized bodies by earth's tidal forces. *Planetary and space science*, 46(2): 311–322, 1998.

William F Bottke Jr, Alberto Cellino, Paolo Paolicchi, and Richard P Binzel. An overview of the asteroids: The asteroids iii perspective. *Asteroids III*, 1:3–15, 2002.

Clark R Chapman. Asteroid collisions, craters, regoliths, and lifetimes. In *NASA Conference Publication*, volume 2053, pages 145–160, 1978.

Alan W Harris and Dmitrij F Lupishko. Photometric lightcurve observations and reduction techniques. In *Asteroids II*, volume 1, pages 39–53, 1989.

Robert Jedicke, Jeffrey Larsen, and Timothy Spahr. Observational selection effects in asteroid surveys and estimates of asteroid population sizes. *Asteroids III*, pages 71–87, 2002.

NASA JPL. Neo groups, 2014a. URL `http://neo.jpl.nasa.gov/neo/groups.html`.

NASA JPL. Absolute magnitude (h), 2014b. URL `http://neo.jpl.nasa.gov/glossary/h.html`.

Ettore Perozzi, Alessandro Rossi, and Giovanni B Valsecchi. Basic targeting strategies for rendezvous and flyby missions to the near-earth asteroids. *Planetary and Space Science*, 49(1):3–22, 2001.

Petr Pravec and Alan W Harris. Fast and slow rotation of asteroids. *Icarus*, 148(1): 12–20, 2000.

Petr Pravec, Alan W Harris, and Tadeusz Michalowski. Asteroid rotations. *Asteroids III*, 113, 2002.

Derek C Richardson, William F Bottke Jr, and Stanley G Love. Tidal distortion and disruption of earth-crossing asteroids. *Icarus*, 134(1):47–76, 1998.

Daniel J Scheeres, Steven J Ostro, Robert A Werner, Eric Asphaug, and RS Hudson. Effects of gravitational interactions on asteroid spin states. *Icarus*, 147(1):106–118, 2000.

Daniel J Scheeres, F Marzari, and A Rossi. Evolution of neo rotation rates due to close encounters with earth and venus. *Icarus*, 170(2):312–323, 2004.

Eugene M Shoemaker, JG Williams, EF Helin, and RF Wolfe. Earth-crossing asteroids: Orbital classes, collision rates with earth, and origin. *Asteroids*, 1:253–282, 1979.

Grant H Stokes, Jenifer B Evans, and Stephen M Larson. Near-earth asteroid search programs. *Asteroids III*, 1:45–54, 2002.

Yu Takahashi, Michael W Busch, and DJ Scheeres. Spin state and moment of inertia characterization of 4179 toutatis. *The Astronomical Journal*, 146(4):95, 2013.

Kevin J Walsh and Derek C Richardson. Binary near-earth asteroid formation: Rubble pile model of tidal disruptions. *Icarus*, 180(1):201–216, 2006.

Appendix

A manosCurveFit System Dependencies

This software was developed and tested on Python 2.7.1, and imports from the following typically pre-installed packages: *operator, os, time, sys*, *string*, and *cmd* and the following typically non-pre-installed packages: *lmfit, matplotlb, numpy* and *uncertainties*.

The latter set of packages are commonly used for scientific applications and stable builds should be easily found.

B manosCurveFit Input, Evaluation, and Output Methods

The software handles data input by reading text files and storing user-defined data columns as numpy arrays in a *lightCurveData* object. Evaluation is handled by the *fitData* function, which utilizes *lmfit*'s minimization routine with free parameters given as Parameter object inputs. Output is handled by the *outputResults* function, which has options to display results in various ways.

B.1 fitInfo Specification

Keyword	Arguments	Meaning
FILES	integer	number of data files for this object (used as a check)
GUESS	string, then 1 or 3 integers	see Guess Specifications section, below
HARDMAXPERIOD	float or int	hard maximum period to not search above
HARDMINPERIOD	float or int	hard minimum period to not search below
OFFSET	string	starts a series of night/offset pairs used by the string specifying the dataset
ENDOFFSETS	N/A	ends the series of offsets (required if OFFSETS are used)

Table 5: fitInfo keywords (all keywords are optional)

Example fitInfo File:

```
FILES 2
# method min max step
GUESS range 14 18 0.25
HARDMAXPERIOD 13
HARDMINPERIOD 20
OFFSET Elisa\elisa_mine_standard.txt
1 0.0
2 -0.04
3 0.464
ENDOFFSETS
OFFSET Elisa\elisa_his_standard.txt
1 -0.324
2 -0.257
3 -0.237
4 -0.194
5 -0.223
6 -0.321
7 -0.246
8 -0.372
9 -0.15
ENDOFFSETS
```

B.2 Guess Specification

Three different ways to specify initial guesses at the period value (in hours) exist.

- range (3 floats or ints) - a range of guesses will be used, following the convention min, max, and step size
  - Example: `GUESS RANGE 0.1 5.5 0.25`
- single (1 float or int) - one initial guess will be used
  - Example: `GUESS SINGLE 2`
- None - if the GUESS line is excluded, an interval from 15 minutes to 5 times the observing window will be used (see section on fitData)

B.3 Command Line Interface

Descriptions of all command line options

- `exit` (no arguments) - exits the program
- `fit` (names of objects to be fit, separated by spaces- must match folder names in the Data directory) - runs a fit on the objects specified, regardless of whether or not they have already been processed
  - Example: `fit Martes Elisa`
- `fitAll` (no arguments, or `'redo'`) - runs fits on all objects in the Data directory that do not have an existing light curve plot; if the `'redo'` argument is provided, all plots are fitted, regardless of any existing fits
- `setFitOptions` (option and value arguments) - sets options used in the fitting routine; multiple options may be set at once
  - `minOrder` (non-negative integer argument) - sets the minimum order to be used in the Fourier fit; default is 2
  - `maxOrder` (non-negative integer argument greater than minOrder) - sets the maximum order to be used in the Fourier fit; default is 6
  - `timer` (boolean) - turns a fitting timer on or off, which measures the amount of time required for each fit, generally for diagnostic purposes
    - Example: `setFitOptions minOrder 3 maxOrder 5 timer true`
- `setOutputOptions` (option and boolean setting arguments) - sets options used in the program output; multiple options may be set at once; all options take booleans
  - `printReport` - whether or not to print the fitting report on the console (default is True)

- `saveReport` - whether or not to save the fitting report to the object's directory (default is True)
- `plotFullPeriod` - whether or not to plot the full period as determined by the model; if not, the model will only plot up to the available data (default is True)
- `plotErrorBars` - whether or not to plot the error bars on the data (default is True)
- `phaseFoldData` - whether or not to phase fold the data and model (default is True)
- `plotResiduals` - whether or not to plot the residuals of the data as a subplot of the light curve (default is True)
- `plotPeriodErrors` - whether or not to plot the mean RMS values the errors as a function of the period attempted (default is True)
- `showPlots` - whether or not the show the plots (default is False); the plots will always be saved to the object's directory

- `showObjects` (no arguments) - lists the object subdirectories found under Data

C manosCurveFit Class and Function Specifications

C.1 The `lightCurveData` Class

class `lightCurveData`(objectName, fileNamesAndFormat[, offsetsList = None])

Creates a lightCurveData object which is used to read in and manipulate the dataset.

Parameters

- **objectName** (string) - name of the object associated with the dataset
  - Example: 'Spartacus20090130'

  - Stored in lightCurveData.name

- **fileNamesAndFormat** (dictionary of dictionaries) - names of text files to be read in, along with the associated column definitions in the data (format specification)

  - Example:

```
fileName = 'Spartacus20090130_MANOS.txt'
# list of lists specifying ['property',column] in the text file
formatSpec = [['night',0],['jd',3],['diffMag',6],['magErr',7]]
fileNamesAndFormat = {fileName:formatSpec}
```

  - Multiple key/value pairs may be used when multiple text files are to be used

  - `'jd'` (Julian date), `'diffMag'` (differential magnitude), and `'magErr'` (magnitude error) must be specified to run the program, additional properties may also be stored in the `lightCurveData` object

  - Remember that Python indexes from zero, so the left-most column in the text file is column 0

  - Any white space in the text file is considered a delimiter (leading and trailing white space is ignored)

  - Stored in lightCurveData.data

- **offsetsList** (list of dictionaries, `None` = no offsets) - offsets associated with nights in each text file

  - Example: [{1:0.0,2:-0.04,3:0.464}]

  - Key/value pairs must be int/float pairs, where the key is the night number, and the value is the offset

- Multiple dictionaries may be used when multiple text files are to be used- when this is done, the order of these dictionaries must correspond to the order of the files names and specifications used in `fileNamesAndFormat`
- Keys may be repeated as long as they are in different dictionaries
- `'night'` property must be specified in the format to use offsetsList
- **If more than one night is used for any target, all data must have associated night and offset values**
  * The only case where offsets are not necessary is if the entire dataset came from a single night

C.2 The `fitData()` Function

`fitData`(lightCurveData, fitOptions, method = None[, periodGuess = None[, hardMinPeriod = None[, hardMaxPeriod = None]]])

- **lightCurveData** (lightCurveData object)
- **fitOptions** (dictionary) - the options used in calculating the fit, as specified in `setFitOptions` (see Command Line Interface)
  - `orderMin` - minimum m value to be attempted in the Fourier model, as outlined in the Fitting Rationale section (default is 2)
  - `orderMax` - maximum m value to be attempted in the Fourier model, as outlined in the Fitting Rationale section (default is 6)
  - `timer` - whether or not to measure the amount of time it takes to fit the model (default is False)
- **method** (string) - method to be used for traversing the search space of periods: `None`, `'single'` or `'range'`; supplied by the fitInfo file, when available

  - when method is `None`, a maximum recoverable period is estimated for up to 5 times the observing window; periods are checked at 15 minute (0.25 hour) intervals; periodGuess is ignored in this case
  - when method is `single`, periodGuess must be provided as an int or a float, which serves as the only initial period used in the minimization
  - when method is `range`, periodGuess must be provided as a three-element list of `[start, stop, step]` integers or floats, which is then automatically converted into a list of initial periods for minimization

- **periodGuess** (int or float or three-element list of ints or floats) - the initial period used for minimization, given in hours; this provides a starting point for the the period parameter, which does not remain fixed during the minimization; supplied by the fitInfo file, when available

- **hardMinPeriod** (int or float) - the hard lower limit for the period fitting, no period below this value will be attempted in the evaluation; supplied by the fitInfo file, when available

- **hardMaxPeriod** (int or float) - the hard upper limit for the period fitting, no period above this value will be attempted in the evaluation; supplied by the fitInfo file, when available

Returns (bestFit, bestOrder, periodsTested, periodErrors), where bestFit is a Minimizer object, bestOrder is an int, and periodsTested and periodErrors are corresponding lists of floats.

C.3 The `outputResults()` Function

`outputResults`(fit, m, lightCurveData, outputOptions[, periodErrors = None])

- **fit** (Minimizer object) - the bestFit object returned by `fitData()`

- **m** (int) - the bestOrder returned by `fitData()`

- **lightCurveData** (lightCurveData object) - the lightCurveData object used for this run

- **outputOptions** (dictionary) - the options used in displaying and saving the results of the run, as specified in `setOutputOptions` (see Command Line Interface)

- **periodErrors** (n by 2 list of lists) - when provided, a second figure will be plotted showing the mean RMS of the residuals as a function of period